RSC Advances

PAPER

View Article Online
View Journal | View Issue

Cite this: *RSC Adv.*, 2022, **12**, 17505

Layer-by-layer coating of MIL-100(Fe) on a cotton fabric for purification of water-soluble dyes by the combined effect of adsorption and photocatalytic degradation

Suhyun Lee,[a] Soyeon Ahn,[b] Halim Lee [b] and Jooyoun Kim *[b]

Efforts have been made for sustainable development of adsorbents to purify organic contaminants from wastewater. In this study, a MIL-100(Fe) based textile that acts as a reusable adsorbent and photocatalytic agent was developed by synthesizing MIL-100(Fe) onto a cotton fabric by the layer-by-layer (LBL) process using water-based solutions. As the number of LBL cycles increased, the add-on's of MIL-100(Fe) showed a drastic increase up to 8 cycles, then showed gradual increases with further treatments. The overall adsorption performance was enhanced with the increased MIL-100(Fe) add-on's, but the specific adsorption efficiency per unit mass of MIL-100(Fe) was reduced as the LBL cycles increased, implying the reduced average adsorption efficiency with a thicker coating. To examine the reusability of the adsorbent, desorption efficiency of RhB was measured. The desorption after the first-time adsorption was not efficient due to the strong binding inside the pores. For the later cycles of adsorption–desorption, desorption occurred more efficiently, probably because RhB molecules were adhered mostly at the outer surface of the MOF layer. Simultaneously, MIL-100(Fe)@cotton demonstrated the photocatalytic degradation performance against RhB in the presence of H_2O_2 by the Fenton reaction. With the combined effect of adsorption and photodegradation, the developed fabric attained 96% removal efficiency for RhB dissolved in water. This study demonstrates an environmentally responsible process of developing a MIL-100(Fe) coated fabric that is readily available for effective removal of organic foulants in water. This fabrication method can be applied as a scalable manufacturing of metal–organic framework-based photocatalytic adsorbent textiles.

Received 2nd May 2022
Accepted 9th June 2022

DOI: 10.1039/d2ra02773a

rsc.li/rsc-advances

1. Introduction

The textile industry generates a large amount of wastewater during the dyeing process. Organic dyes, as one of the most common pollutants in wastewater, are chemically stable and usually non-biodegradable in water, disrupting the aquatic ecosystem by impeding the penetration of sunlight and oxygen.[1,2] Up to date, various technologies have been used to remove dyes from wastewater, including chemical, biological, and physical methods.[3] Among them, the physical method has been used most frequently for its efficiency and convenience, where this method employs a porous material such as activated carbon and zeolite to adsorb and separate the foulants.[4] However, purification of the aquatic environment by the conventional single-use filter leaves a big challenge of generating secondary environmental waste, thus creating another source of pollution.[1]

Metal–organic frameworks (MOFs) as a new class of porous materials with a large surface area and open framework have attracted considerable attention.[5,6] They present superior performance compared with other traditional adsorbent materials used in filtration and separation. In particular, MOFs can be used as photocatalysts and adsorbents simultaneously for the removal of organic contaminants from water.[4,7,8] However, direct usage of powdery MOF faces challenges from the perspective of efficiency and reusability.[9] For example, when MOF powder is used as an adsorbent, it is difficult to recover the particles after use, and the unrecovered particles remain in water as secondary contaminants. Therefore, incorporating MOFs in a stable substrate, rather than using as powdery form, may be favored in such an application. Since the fibrous materials have sufficient strength and flexibility, researches have been conducted applying MOFs onto the textile materials by various fabrication methods.[10–13]

Among the methods, the layer by layer (LBL) approach has been used to attain a uniform coating by immersing the fabric

[a]*Department of Fashion Design, Jeonbuk National University, Jeonju, 54896, Republic of Korea*

[b]*Department of Textiles, Merchandising and Fashion Design, Seoul National University, Seoul, 08826, Republic of Korea. E-mail: jkim256@snu.ac.kr*

substrate in a metal ion solution and then an organic ligand solution in sequence.[14–16] This LBL method, which proceeds at a relatively low temperature, is suitable for manufacturing the fabric-based MOF adsorbent, used for removal of organic pollutants existing in liquid. Da Silva Pinto *et al.*[17] modified a cellulose fabric into an anionic surface through carboxymethylation, and the MOF (HKUST-1) was chemically bonded to the cellulose surface by the LBL procedure at room temperature. Rubin *et al.*[18] fabricated a carboxymethylated cotton fabric to attain nucleation sites for MOF growth, and then attached MOFs by the LBL approach using a mechanical dip coater. As a result, a durable and flexible MOF-grown cotton fabric (MOF@cotton) was manufactured, displaying a uniform coating of MOFs with distinct morphology. Schelling *et al.*[19] reported on the successful functionalization of cotton fabrics with a water-stable MOF, UiO-66, under mild solvothermal condition (80 °C), and its ability to adsorb and degrade water micropollutants was demonstrated. However, studies of MOF-treated fabrics so far have used toxic organic solvents such as dimethylformamide and dimethylacetamide to dissolve metal ions and organic ligands. In addition, ethanol or methanol has been commonly used to remove those toxic solvents after the synthesis of MOF. Moreover, in order to firmly bind the MOFs to the fabric, functional groups are commonly imparted on the fabric surface through pre-treatment such as mercerization or carboxymethylation. Not only that this procedure is rather complicated, but also it is concerning to use toxic solvents in the procedure, which would eventually need wastewater treatment. Therefore, more environmentally responsible production needs to be considered.

This study aims at developing a fabric-based MOF adsorbent for removal of water-soluble organic dyes, by employing LBL method without using organic solvents in production. For this purpose, MIL-100(Fe) was selected as a MOF adsorbent as it is stable in water and minimally toxic to human. As a substrate, a cotton fabric was chosen as its mechanical strength in wet state is high. Also, its –OH groups would work as the binding sites of MOFs without prior treatment. The dye adsorption performance of MIL-100(Fe) treated cotton fabric (MIL-100(Fe)@cotton) was investigated with the varied number of LBL cycles. The desorption efficiency of adsorbed dyes on MIL-100(Fe)@cotton was evaluated to discuss the reusability of the developed adsorbent fabric. The photocatalytic performance under visible light was evaluated to investigate the effect of dual action of adsorption and photodegradation on the dye removal performance in water. This study intends to provide an informational discussion on the scalable and eco-friendly manufacturing method of MOF-based adsorbent textiles that can remove water-soluble contaminants by both effects of adsorption and photocatalytic degradation.

2. Experiments

2.1. Materials

For synthesis of MIL-100(Fe), iron(III) chloride hexahydrate ($FeCl_3 \cdot 6H_2O$, 99%, Wako, Japan) was used for the metal ion, and trimesic acid (H3BTC, 98%, Alfa Aesar, USA) was used for the organic ligand. Sodium carbonate anhydrous (Na_2CO_3, 99%, Junsei, Japan) was used as a scouring agent. Rhodamine B (RhB, SCI Seoul Chemicals, Korea) was used as a model foulant to evaluate the adsorption and photodegradation performance of the MIL-100(Fe)@cotton. Ethanol (EtOH, 99.9%, Daejung, Korea) was used as a solvent of desorption test. All chemicals were in the analytical grade and used without prior treatment.

Woven fabric with 100% cotton was used as a substrate. Its weight and thickness were 123.3 g m^{-2} and 0.35 mm, respectively. Cotton fabric was used after scouring. Fabric specimens were immersed in a 1% Na_2CO_3 solution prepared with a liquid ratio of 1 : 50 at 70 °C for 30 min, rinsed with distilled water 10 times or more, and dried at room temperature.

2.2. Fabrication of MIL-100(Fe)@cotton fabrics

The metal ion solution, $FeCl_3 \cdot 6H_2O$ in water, was prepared in 15 mM. The organic ligand solution, H_3BTC in water was prepared in 10 mM. The layer by layer (LBL) process followed the procedure shown in Fig. 1. The cotton fabric in 10 × 10 cm was immersed in a 100 mL of organic ligand solution for 30 min and washed with distilled water for 5 min. Subsequently, the washed fabric was immersed in a 100 mL of metal ion solution for 15 min and then washed with distilled water again. This procedure was considered as one LBL cycle. This process was repeated 2, 4, 6, 8, 10, and 12 times. After the LBL process, the sample was dried in an oven (Wiseoven WOF-105, Daihan Scientific, Seoul, Korea) at 60 °C for 12 h.

2.3. Characterization

A field emission scanning electron microscopy (FE-SEM, JSM-7800F Prime, JEOL Ltd, Tokyo, Japan) was performed to observe the surface of the cotton fabrics after growing MIL-100(Fe) by LBL process. To prevent the charge-up phenomenon, samples were sputter-coated with platinum prior to examination. A sputter coater (108 auto, Cressington Scientific Inc., Hertfordshire, UK) was used at a current of 20 mA for 120 s.

The add-on's of MIL-100(Fe) per unit area with the number of LBL cycles were calculated following eqn (1) by measuring the weight before and after the processing: where W_a is the dried weight of sample after the LBL process (g), W_b is the dried weight of samples before the LBL process (g), and A is the area of the sample (m^2).

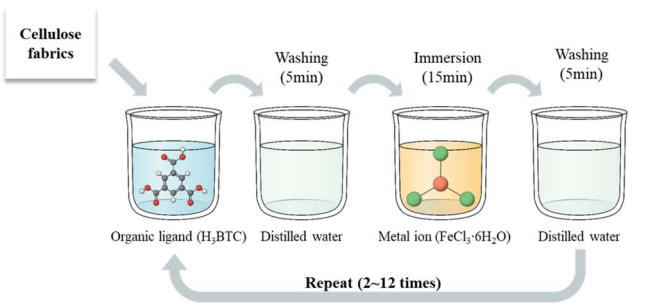

Fig. 1 LBL process to fabricate of MIL-100(Fe)@cotton process.

$$\text{MIL-100(Fe) add-on } \left(\text{g m}^{-2}\right) = \frac{W_a - W_b}{A} \quad (1)$$

Changes in the crystal structure was analysed by the X-ray diffraction (XRD). The XRD analysis was performed on an X-ray diffractometer (D8 Advance, Bruker, Bremen, Germany) using Cu Kα ($\lambda = 1.54$ Å, 40 kV, 40 mA) as the X-ray source, at the scanning rate of 0.4° s^{-1} in the range from 5° to 40°. The X-ray diffraction pattern was analyzed using DIFFRAC.SUITE software. The mechanical property of MIL-100(Fe)@cotton was evaluated by the tensile test. The tensile strength was measured using a universal testing machine (5ST, Tinius Olsen Ltd, Surrey, UK) with an extension rate of 10 cm min^{-1}. The sample was prepared with a size of 2.5 cm × 15 cm and measured in the warp and weft directions.

2.3.1. Dye removal by adsorption and photodegradation. RhB was used as a target dye pollutant because it is widely used in the textile industry.[20,21] Removal efficiency of RhB dye was evaluated by immersing a 3 cm × 3 cm sample of MIL-100(Fe)@cotton in 50 mL of aqueous RhB solution with a concentration of 10–40 mg L^{-1}. The sample-immersed solution was stirred in a shaking water bath (LB-SW060, LabKorea, Namyangju, Korea) at 20 °C and 120 rpm.

The absorbance was measured by extracting 200 μL solution until the adsorption equilibrium was reached. The optical density of the solution was measured using a spectrophotometer (Synergy H1, BioTek, VT, USA) at 553 nm, which is the maximum absorption wavelength of RhB.

The overall RhB removal efficiency and the specific removal efficiency per unit mass of MOF were calculated according to eqn (2) and (3): where C_0 is the initial concentration of RhB solution (mg L^{-1}), C_t is the concentration of RhB solution at time t (mg L^{-1}), V is the volume of the solution (L), and m is the weight of MIL-100(Fe) (g).

$$\text{Overall removal efficiency } (\%) = \left(1 - \frac{C_t}{C_0}\right) \times 100 \quad (2)$$

$$\text{Removal efficiency per gram of MOF } \left(\frac{\text{mg}}{\text{g}}\right) = \frac{(C_0 - C_t)V}{m} \quad (3)$$

As MIL-100(Fe) may show both photocatalytic and adsorption effects, the adsorption effect of MIL-100(Fe)@cotton was evaluated in dark condition, using eqn (2) and (3).

When it is tested under the light irradiation, the removal efficiency was regarded to come from the combined effect of adsorption and photocatalytic reaction. The Fenton activity was tested with and without light irradiation. For the test of Fenton reaction, 1 mL of H_2O_2 was mixed into the MIL-100(Fe)-added dye solution. As a light source, F20T12/65 6500 K lamp (white LED, 20 W, GretagMacbeth), artificial daylight, was used. During the test, the solution was stirred for a homogeneous reaction. Two control tests were run with (1) untreated cotton fabric with light and (2) H_2O_2 only with light.

2.3.2. Desorption and reusability evaluation. The feasibility for regenerating the exhausted MIL 100(Fe)@cotton by RhB adsorption was evaluated by rinsing the used adsorbent in ethanol for desorption of adsorbed dyes. The adsorption equilibrium was reached within 24 h. After 24 h adsorption, the sample was dried at 30 °C. The dried sample was immersed in 50 mL of ethanol, stirred in a water bath at 20 °C and 120 rpm, and washed by ethanol. During the desorption process, a 200 μL of the rinsing solution was extracted at 1 h interval until the desorption equilibrium state was reached. The optical density of the solution was measured using a spectrophotometer at 543 nm, which is the maximum absorption wavelength of RhB solution in ethanol. The desorption efficiency was calculated according to eqn (4): where C_a is the concentration of adsorbed dye (mg L^{-1}) and C_d is the concentration of desorbed dye (mg L^{-1}).

$$\text{Desorption efficiency } (\%) = \frac{C_d}{C_a} \times 100 \quad (4)$$

Reusability was discussed based on the repeated tests of adsorption and desorption. For this test, re-adsorption and re-desorption were performed following the same method as above. After the desorption process, the sample was dried at 30 °C to evaporate ethanol and used for re-adsorption evaluation.

3. Results and discussion

3.1. Appearance and add-on of MIL-100(Fe)@cotton with varied LBL cycles

Fig. 2 shows the cotton fabric on which MIL-100(Fe) was grown by LBL process. It is visually shown that the MIL-100(Fe)@cotton developed darker colors as the number of LBL cycles increased.[20] Darker shades of treated fabrics demonstrate that more layers of MIL-100(Fe) crystals were attached to the fabric as the LBL cycles increased. The color change was less noticeable after L8.

The morphology of fabrics was observed by SEM (Fig. 3) to investigate the growth of MIL-100(Fe) on cotton with the number of LBL cycles. The surface of the untreated cotton fabric showed the fibril structure with relatively smooth surface. The MIL-100(Fe)@cotton showed MIL-100(Fe) particles attached to the fiber surface. When the number of LBL was 2 cycles (Fig. 3(b) and (f)), very few MIL-100(Fe) particles were observed. As the number of LBL was increased to 10 cycles (Fig. 3(d) and (h)), the MIL-100(Fe) particles grew large enough to completely cover the fiber surface. With L10, a large amount of MIL-100(Fe) was uniformly and densely grown on the surface of the cotton fibers, and this observation is consistent with the study by Lu *et al.*[21]

The dense growth of MIL-100(Fe) on cotton fabric demonstrates that the organic ligands and metal ions effectively formed MIL-100(Fe) crystals on cotton surface. Fig. 4 shows a synthesis procedure for the layer-by-layer MIL-100(Fe) growth on the cotton fabric. When a cotton fabric is immersed in an organic ligand solution, the organic ligand binds to the

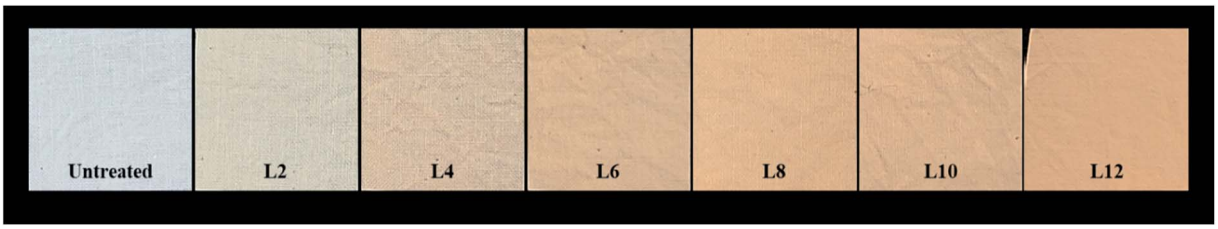

Fig. 2 Photo of MIL-100(Fe)@cotton samples.

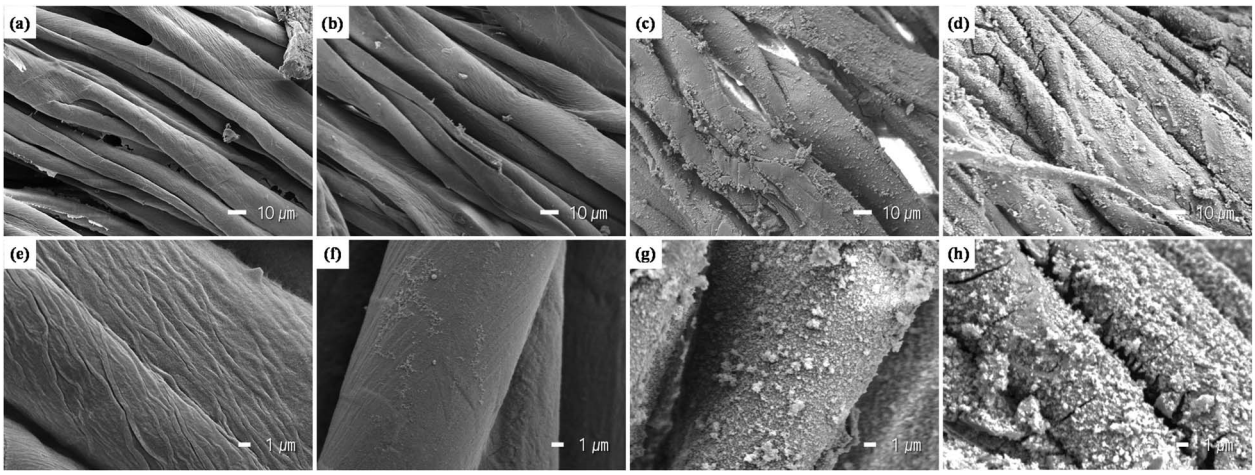

Fig. 3 Appearance of MIL-100(Fe)@cotton at ×1000 and ×5000 magnifications: (a) and (e) untreated; (b) and (f) L2; (c) and (g) L6; (d) and (h) L10.

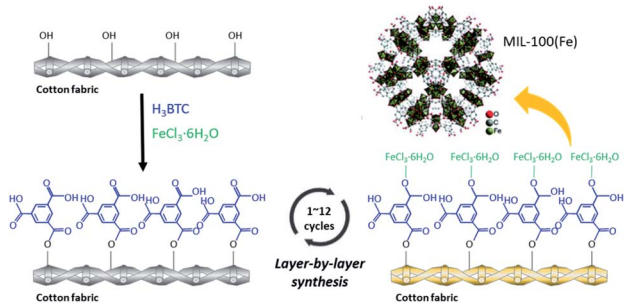

Fig. 4 Principle of the layer-by-layer process of MIL-100(Fe) growth on cotton fabric.

hydroxyl group of the cotton cellulose, and then the bound organic ligand reacts with metal ions to grow the MOFs. When LBL process is repeated, more MOFs can be uniformly grown on the fiber surface due to the participation of the remaining hydroxyl groups of the cotton fabric. Also, the rough surface area of cotton fabric consisting of staple fibers is advantageous to provide reactive sites to attach MIL-100(Fe) precursors.[22]

The add-on amount of the MIL-100(Fe)@cotton with the number of LBL cycles are presented in Fig. 5. The add-on's (% weight change by the growth of MIL-100(Fe)) for different treatments are as the following: L2, 0.57 g m^{-2}; L4, 4.97 g m^{-2}; L6, 10.52 g m^{-2}; L8, 16.54 g m^{-2}; L10, 18.45 g m^{-2}; L12, 20.01 g m^{-2}. As the number of LBL increased, the add-on increased linearly up to L8, and the add-on increase became gradual thereafter. This is due to the limited number of remaining hydroxyl groups that can further react with organic ligands for L8 or more cycles of treatments.

3.2. Chemical and physical properties of MIL-100(Fe) @cotton

To confirm the MIL-100(Fe) crystal formation on the cotton fabric, X-ray diffraction (XRD) measurements were carried out over the diffraction angle (2θ) of 5–40°. Fig. 6 shows the XRD patterns from MIL-100(Fe) powder, cotton fabric, and MIL-

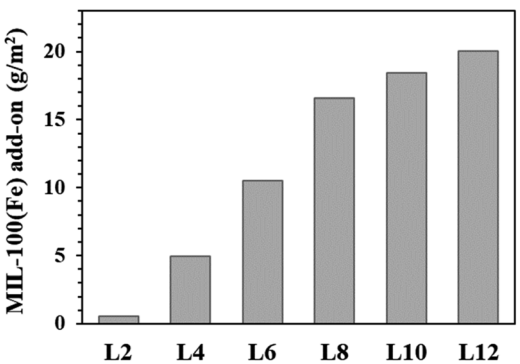

Fig. 5 Add-on of MIL-100(Fe) on cotton fabric with different LBL cycles.

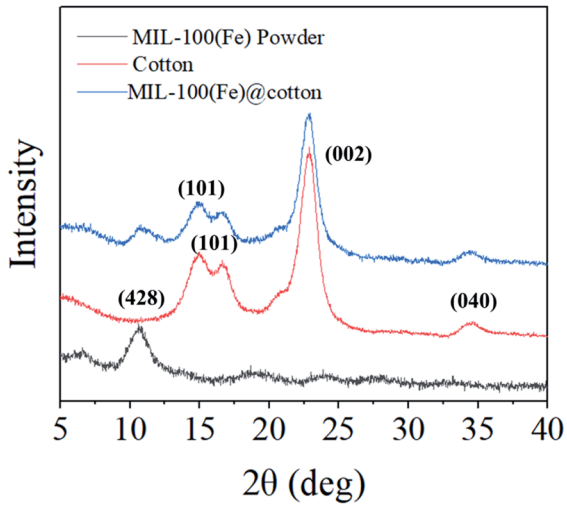

Fig. 6 XRD patterns of untreated cotton, MIL-100(Fe) powder, and MIL-100(Fe)@cotton (L6).

100(Fe)@cotton (L6). In the XRD pattern of cotton fabric, the peaks located near 14.9°, 16.7°, 22.8°, and 34.6° are the characteristics of (101), (101), (002), and (040) reflections of cellulose I.[23] The characteristic peaks at 11.0° in the XRD pattern of MIL-100(Fe) powder corresponded to the (428) plane of the MIL-100(Fe).[14] This diffraction peaks of MIL-100(Fe) was detected also from MIL-100(Fe)@cotton, which affirmed the successful growth of MIL-100(Fe) on the cotton fabric.

The tensile strength and elongation of MIL-100(Fe)@cotton was measured to examine the change of mechanical properties after growth of MIL-100(Fe) (Fig. 7). The tensile strength was: 236 ± 7 kg cm^{-2} in warp direction and 214 ± 5 kg cm^{-2} in weft direction for the untreated cotton fabric; 223 ± 9 kg cm^{-2} in warp direction and 220 ± 10 kg cm^{-2} in weft direction for MIL-100(Fe)@cotton (L6), respectively. The elongation was: 32.3 ± 0.9% in warp direction and 34.5 ± 0.9% in weft direction for untreated cotton fabric; 25.2 ± 1.0% in warp direction and 27.6 ± 0.8% in weft direction for MIL-100(Fe)@cotton, respectively.

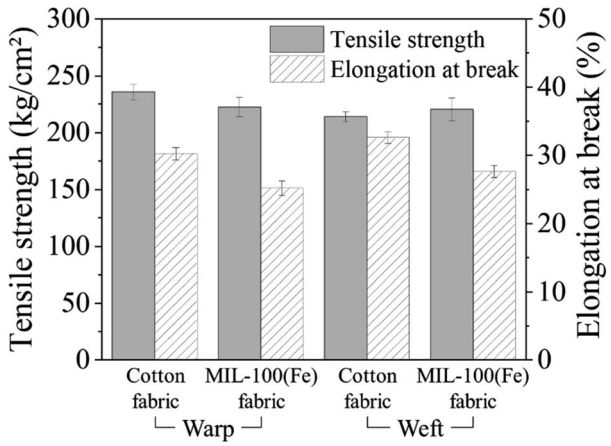

Fig. 7 Tensile strength and elongation of cotton fabric with and without MIL-100(Fe) coating (L6).

From the results, the tensile strength did not change much, but the elongation decreased by about 20% after the MOF coating. This is because MIL-100(Fe) filled the space between the fibers, decreasing the mobility of the fibers.[24] The attached MIL-100(Fe) formed a layer on a fabric surface and fixed the MIL-100(Fe) and fibers; as a result, the yarns of MIL-100(Fe)@cotton were not loosened as much as those of cotton fabric, when immersed in dye solution for 60 h (L10 from Fig. 8(b)).

3.3. Adsorption of MIL-100(Fe)@cotton with varied LBL cycles

The adsorption performance of MIL-100(Fe)@cotton on the water-soluble organic dye, RhB, was observed. The RhB adsorption of untreated cotton fabric was less than 0.4 mg L^{-1}, which was less than 2% of the initial RhB concentration (20 mg L^{-1}). From the result, the control fabric does not show significant adsorption performance, and hardly affects the adsorption performance of the MIL-100(Fe)@cotton.

To examine the adsorption performance with LBL cycles, the overall adsorption (%) for 3 cm × 3 cm fabric and the specific adsorption efficiency per g of MIL-100(Fe) were measured in an RhB aqueous solution of 20 mg L^{-1} concentration for 24 h. The functional group of MIL-100(Fe) can induce various molecular interactions such as van der Waals interaction, π–π interactions, and hydrogen bonding.[25–27] MIL-100(Fe) possesses two sets of mesoporous cages (25 and 29 Å) that are accessible through two microporous windows (5 and 9 Å) and corresponding large Langmuir surface areas.[28,29] Those adsorption sites allowed π–π interactions between the benzene rings in RhB molecule and MIL-100(Fe). Moreover, the possible interactions between the Lewis base –N(C_2H_5)$_2$ in RhB and the Lewis acid Fe sites of MIL-100(Fe) can also play an important role.[30] At the solution pH ≥ 5, the surface of MIL-100(Fe) is negatively charged.[31] In this study, the adsorption performance was evaluated in an aqueous solution at pH 7. Thus, the cationic dye, RhB, should be adsorbed to the MIL-100(Fe)@cotton mostly by the electrical attraction.

From Fig. 9, the adsorption (%) increased linearly as the number of LBL cycles increased, due to the increased amount of MIL-100(Fe). However, the adsorption efficiency increased up to L8, reaching the maximum of 80.9%. The concentration of the adsorbed dye plateaued thereafter, probably because the outermost surface area of the MIL-100(Fe)@cotton was not

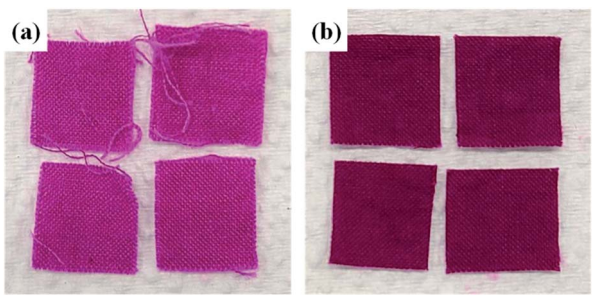

Fig. 8 Appearance of MIL-100(Fe)@cotton after immersing in RhB solution for 60 h: (a) L2, and (b) L10.

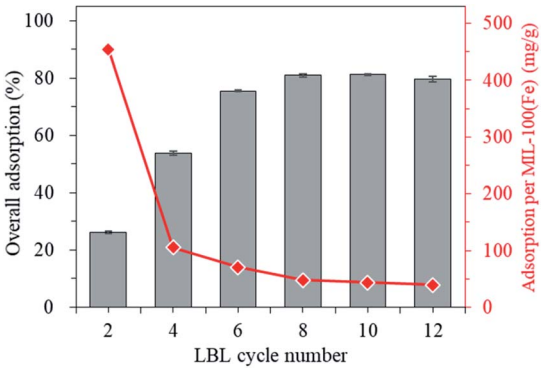

Fig. 9 Adsorption of RhB dye on MIL-100(Fe)@cotton with varied LBL cycles.

further increased from L8. When all adsorption sites of the MIL-100(Fe)@cotton were occupied by dye molecules, further adsorption hardly occurred due to the repulsive forces between the adsorbed dyes and the free dye molecules present in water.[32]

On the other hand, the specific adsorption efficiency per g of added MIL-100(Fe) decreased as the number of LBL increased. Up to L6, the adsorption efficiency (per g of MIL-100(Fe)) decreased significantly with the increase of MIL-100(Fe) add-on's, but there was no significant difference thereafter. As the LBL cycle increased, the add-on of MIL-100(Fe) increased accordingly; however, it is the outer most layer of MIL-100(Fe) @cotton that contributes to the most of adsorption, leaving the inner layer of MIL-100(Fe) intact of dyes. Thus, the per gram-adsorption efficiency of MIL-100(Fe) decreased as the add-on's increased. The overall adsorption evaluated by the reduction of dye concentration significantly increased from L2 to L6, but the additional performance change thereafter was marginal, as the adsorption sites of the outer most layer of MIL-100(Fe) are fairly well occupied from L6. Since the adsorption in MIL-100(Fe) @cotton occurs mainly at the MOF layer, MIL-100(Fe) should be distributed as much as possible over the surface of the fabric to increase the adsorption capacity.[20,21] However, as the number of LBL cycles increased, the MIL-100(Fe) formed a thicker layer, where the inner layer of MIL-100(Fe) was not available for adsorption.[33] Thus, the add-on was not linearly increased with the LBL cycles. This affected the specific adsorption efficiency per gram of MIL-100(Fe). To sum up, the MIL-100(Fe) attached to the outer most layer of the fabric contributed the most to the adsorption, and the total amount of MIL-100(Fe) added onto the fabric was less important.

Fig. 10 shows the overall adsorption (%) and adsorption efficiency of MIL-100(Fe)@cotton with the RhB concentration after 24 h of adsorption. The overall adsorption gradually decreased as the RhB concentration increased, regardless of the number of LBL cycles (Fig. 10(a)). The overall adsorption (%) was calculated by eqn (2) in dark condition. The higher overall adsorption at the lower RhB concentration is attributed to the sufficient adsorption sites of MIL-100(Fe) compared to the RhB amount in the solution. When the RhB concentration was increased to 40 mg L^{-1}, the overall adsorption decreased as the availability of the adsorption sites of MIL-100(Fe) was reduced.[34]

In all samples, the specific adsorption efficiency per g of MIL-100(Fe) increased as the RhB concentration increased, as shown in Fig. 10(b). This is probably because the amount of MIL-100(Fe) was sufficient to adsorb RhB up to 40 mg L^{-1} concentration. The adsorption efficiency (per g MIL-100(Fe)) was proportional to the RhB concentration, and inversely proportional to the add-on of MIL-100(Fe). L2, which had he smallest MIL-100(Fe) add-on, showed the largest amount of RhB adsorption per unit MIL-100(Fe) mass. When the concentration of RhB solution was increased from 10 mg L^{-1} to 40 mg L^{-1}, the overall adsorption was increased by: 2.19 times for L2; 2.21 times for L4; 2.94 times for L6; 3.10 times for L8; 3.30 times for L10; and 3.19 times for L12. Notably, the overall adsorption did not increase at the higher dye concentration for L10 or higher LBL cycles. Thus, L10 was selected as an optimal LBL cycle that demonstrates the highest overall adsorption at the dye concentrations tested in this study (10 mg L^{-1} to 40 mg L^{-1}).

3.4. Desorption and reusability

As consideration of sustainable use of adsorbent material,[35] reusability of the MIL-100(Fe)@cotton was examined by the

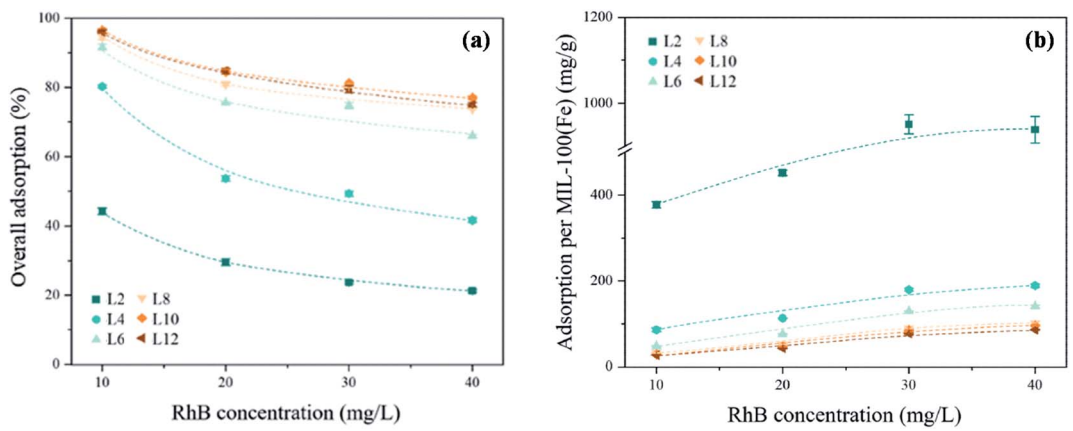

Fig. 10 Adsorption of RhB dye on MIL-100(Fe)@cotton with varied concentrations of RhB solution: (a) overall adsorption (%), (b) specific adsorption per MIL-100(Fe) (mg g^{-1}).

repeated adsorption–desorption processes. This experiment was conducted at 20 mg L^{-1} dye concentration. After the adsorption of RhB for 24 h, the adsorbed sample was immersed in ethanol for 8 h for cleaning, or desorption. For the untreated cotton fabric, the desorbed dye concentration was insignificant, being below 0.1 mg L^{-1}. Therefore, it is considered that the untreated cotton fabric used as the substrate did not have a significant effect on the desorption results of the MIL-100(Fe)@cotton.

Desorption study was conducted for L10 fabric. As shown in Fig. 11(a), a desorption equilibrium reached within 1 h in the first-time desorption, giving desorption efficiency of only 22.3%. The cation dye, RhB would be adsorbed on the interior pores and/or the reactive sites of outer surface on MIL-100(Fe), *via* van der Waals force and electrical attraction.[21] The reason for the low desorption at the first-time is probably because RhB molecules adsorbed in the interior pore of MOF were not easily desorbed by ethanol rinsing (desorption process). The fabric appeared pink even after the desorption, confirming the incomplete desorption of RhB. At the second adsorption, RhB was re-adsorbed about 72.0% and desorbed 76.5% of the adsorbed dye. The second desorption was higher because the re-adsorption mainly occurred on the surface of MIL-100(Fe) as additional layers, with lower binding strength.

Fig. 11(b) shows the results of repeated adsorption and desorption processes up to three times. The overall adsorption performance of MIL-100(Fe)@cotton decreased from 81.2% to 67.7% during three cycles. This is because the adsorbed dye molecules still remained in the sample, without being completely desorbed by the ethanol treatment. However, the specific adsorption efficiency per g of MOF was: 43.4 mg g^{-1} in the first adsorption cycle; 38.9 mg g^{-1} in the second adsorption (after ethanol rinsing); and 36.1 mg g^{-1} in the third adsorption process (after ethanol rinsing). The third-time adsorption efficiency was about 83.2% of the initial adsorption efficiency. The adsorption efficiency was maintained high regardless of the repeated adsorption–desorption processes, indicating the potential applicability of MIL-100(Fe)@cotton as a reusable adsorbent.

3.5. Photodegradation effect

The combined effect of photodegradation and adsorption of MIL-100(Fe)@cotton was evaluated for RhB solution under the light irradiation. Fig. 12 shows the overall RhB removal efficiency by adsorption and/or photocatalytic degradation process for untreated cotton and MIL-100(Fe)@cotton (L10). From the untreated cotton (with light), RhB was barely photolyzed or adsorbed. Also, H_2O_2 itself had no effect on reducing the RhB concentration.

As MIL-100(Fe) could have both photocatalytic and adsorption ability, it was tested with and without light irradiation to discern the adsorption and the photocatalytic-combined effect. Under the dark condition, MIL-100(Fe)@cotton showed 77.2% of removal efficiency by the adsorption of RhB dye. As the addition of H_2O_2 can induce the Fenton reaction, H_2O_2 was added to MIL-100(Fe)@cotton in dark condition; from the result

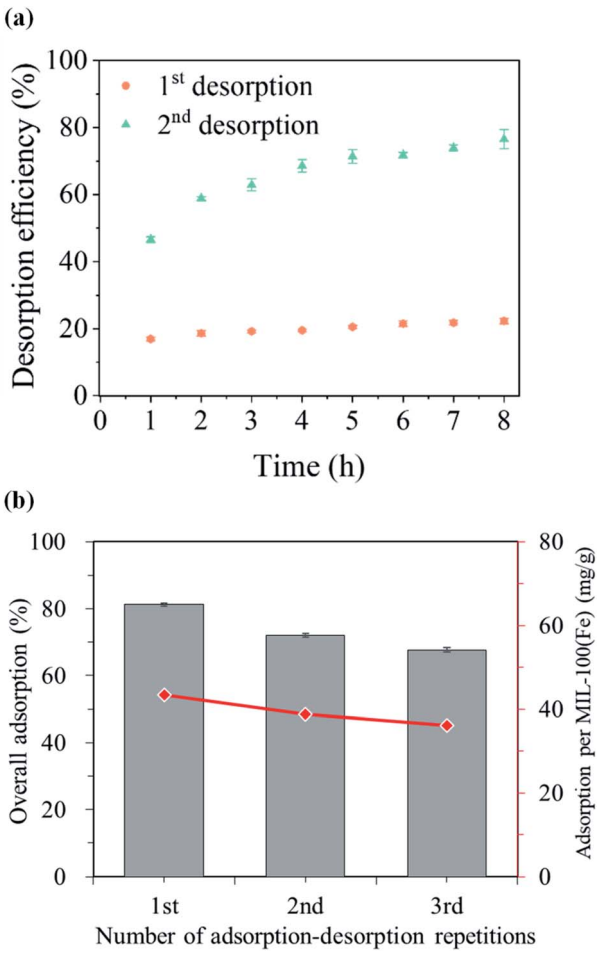

Fig. 11 Desorption and readsorption of RhB dye on MIL-100(Fe)@cotton (L10): (a) desorption efficiency, (b) overall adsorption.

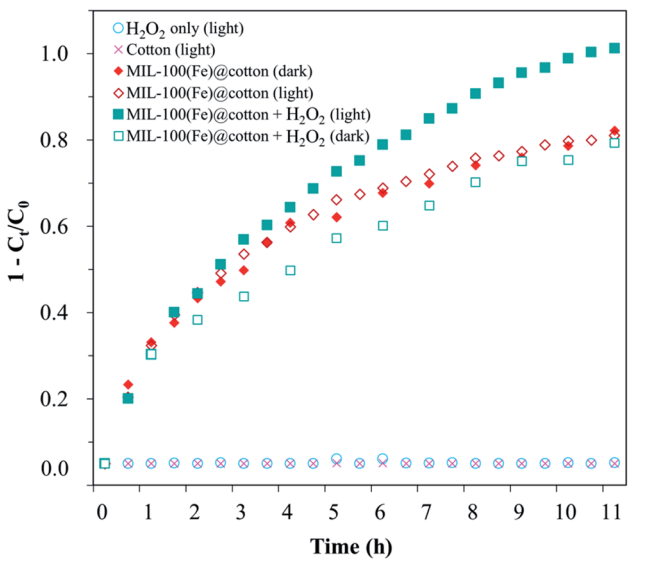

Fig. 12 Adsorption and photocatalytic degradation of RhB dye by MIL-100(Fe)@cotton (L10).

of "MIL-100(Fe)@cotton + H_2O_2 (dark)", it does not seem that effective Fenton reaction had occurred in dark.

Meanwhile, under the light irradiation and with the presence of H_2O_2, the MIL-100(Fe)@cotton demonstrated the improved RhB removal efficiency by the dual action of adsorption and Fenton catalytic degradation. Until 2 h, the RhB concentration was similar regardless of the presence of H_2O_2 and light (with removal rate of about 4 mg h^{-1}) implying that the reduced RhB concentration up to this point is the result of adsorption rather than photocatalytic reaction. After 2 h, the plots began to deviate depending on the addition of H_2O_2. For MIL-100(Fe)@cotton with H_2O_2 addition (under light) demonstrated both adsorption and photodegradation effects, giving 96% reduction of RhB concentration. Notably, the Fenton reaction under dark condition was not efficient, demonstrated by the fact that a similar profile was observed from MIL-100(Fe)@cotton (dark) and MIL-100(Fe)@cotton + H_2O_2 (dark). It appears that the light irradiation was essential in inducing the Fenton oxidation in this experiment.

MOF is constructed of metal cluster which is coordinated to organic ligands, thus the outer orbital of metal acts as the empty conduction band and that of organic ligand acts as the valence band.[36] In MIL-100(Fe) with Fe as central metal, the Fe–O clusters can be excited and make the electron transfer from O^{2-} to Fe^{3+} to form Fe^{2+} and H^+ which can participate in the photocatalytic reaction.[37,38] This reduced Fe^{2+} can initiate the photo-Fenton reaction with H_2O_2. Subsequently, H_2O_2 captures the photo-induced electrons in the MIL-100(Fe) to form hydroxyl radicals and further decompose the organic pollutants.[39–41] MIL-100(Fe) has narrow bandgap of 2.50 eV compared to other metal-based semiconductors such as zinc oxide and titanium oxide.[36,42] The valence band and conduction band edge potentials of MIL-100(Fe) are reported to be −0.65 eV and 1.85 eV.[43] Therefore, MIL-100(Fe) can activate a photocatalytic reaction even under the visible light.[8,9,42] When MIL-100(Fe) is exposed to the light, of which energy is greater than its bandgap, the electron–hole pairs can be formed.[9,36] However, due to the small bandgap, the recombination of electrons and holes occurs easily, prohibiting the proper photocatalytic reaction.[37] In this process, H_2O_2 can inhibit the electron–hole recombination by acting as an electron acceptor,[44] and eventually helps the photocatalytic reaction. In addition, the photo-induced electrons from MIL-100(Fe) can generate hydroxyl radicals by reacting with H_2O_2, granting the oxidation ability to degrade RhB molecules.[9,36,38]

The stability of MIL-100(Fe)@cotton after the photodegradation was investigated by SEM. As shown in Fig. 13, the MIL-100(Fe) particles were adhered well to the cotton surface even after undergoing RhB adsorption and photodegradation processes. In addition, fiber damage by photocatalytic activity was not clearly observed.

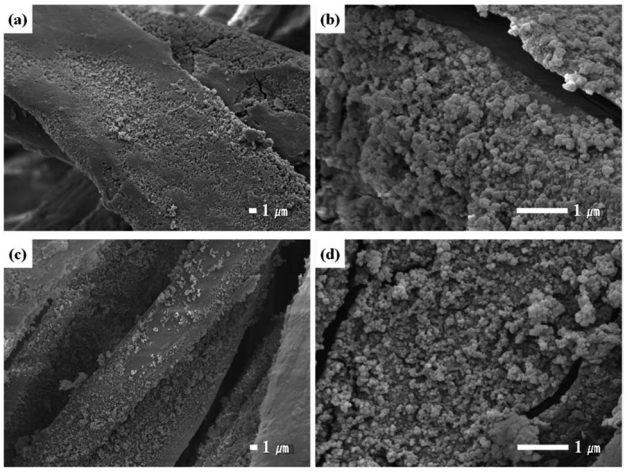

Fig. 13 Appearance of MIL-100(Fe)@cotton at ×3000 and ×20 000 magnifications: (a) and (b) after adsorption of RhB (tested in dark condition); (c) and (d) after photodegradation (tested with H_2O_2 under light).

4. Conclusions

MIL-100(Fe)@cotton was prepared by the layer-by-layer (LBL) process to investigate the applicability of the developed fabric as a reusable adsorbent for liquid purification. The adsorption–desorption properties and photocatalytic ability of MIL-100(Fe)@cotton were evaluated employing rhodamine B (RhB) dye as a water-soluble model contaminant. As the number of LBL cycles increased, the add-on of MIL-100(Fe) increased, forming a uniform coating on the fabric surface. As the LBL cycles increased, the overall adsorption performance against RhB increased. On the other hand, the specific adsorption efficiency per g of MIL-100(Fe) decreased because the outermost layer of MIL-100(Fe) mostly contributed to the adsorption. When the dye concentration increased, the adsorbed amount of RhB was reduced, and the specific adsorption efficiency per unit mass of MIL-100(Fe) tended to increase. This tendency was clearer as LBL cycles increased. Using the treated sample with 10 cycles of LBL (L10), adsorption performance was evaluated with repeated adsorption–desorption processes to examine the reusability of adsorbent material. In the first desorption process, 22% of the adsorbed dye was desorbed, implying that only the molecules weakly adhered at the surface was detached, leaving those inside the pores intact. With 2nd and 3rd adsorption–desorption processes, the desorption efficiency significantly increased, probably because the 2nd and later adsorption occurred mostly at the MOF surface by weaker adhesion force. The MIL-100(Fe) also demonstrated the photocatalytic ability of RhB in the presence of H_2O_2, and the combined effect of adsorption and photocatalytic reaction allowed 96% removal efficiency of RhB.

In this study, an effective photocatalytic adsorbent that allows the removal of water-soluble foulant was developed by the sustainable process without using toxic organic solvents. The results revealed that a thin layer coating of MIL-100(Fe) with large surface area, rather than a thick MOF coating, is advantageous for efficient adsorption of foulants per unit mass of MIL-100(Fe). This study provides an informative discussion on developing a MOF-based water purifying material, which functions by the dual action of adsorption and photocatalytic degradation. The fabrication method investigated in this study can be applied as a scalable manufacturing of MOF-based

photocatalytic adsorbent textiles. Future study is anticipated for examining the applicability of this material to other water contaminants such as phenolic compounds.

Conflicts of interest

The authors declare no potential conflicts of interest with respect to the research, authorship, and/or publication of this article.

Acknowledgements

This work was supported by the National Research Foundation (NRF) of Korea funded by the Korean government (MSIP) (No. 2022R1A2C2003072).

References

1 B. Wang, Z. Xie, Y. Li, Z. Yang and L. Chen, *Macromolecules*, 2018, **51**, 3443–3449.
2 G. Yang, D. Zhang, G. Zhu, T. Zhou, M. Song, L. Qu, K. Xiong and H. Li, *RSC Adv.*, 2020, **10**, 8540.
3 M. T. Yagub, T. K. Sen, S. Afroze and H. M. Ang, *Adv. Colloid Interface Sci.*, 2014, **209**, 172–184.
4 N. M. Mahmoodi, J. Abdi, M. Oveisi, M. A. Asli and M. Vossoughi, *Mater. Res. Bull.*, 2018, **100**, 357–366.
5 T. Islamoglu, Z. Chen, M. C. Wasson, C. T. Buru, K. O. Kirlikovali, U. Afrin, M. R. Mian and O. K. Farha, *Chem. Rev.*, 2020, **120**, 8130–8160.
6 S. Ramanayaka, M. Vithanage, A. Sarmah, T. An, K. H. Kim and Y. S. Ok, *RSC Adv.*, 2019, **9**, 34359.
7 S. Shams, W. Ahmad, A. H. Memon, Y. Wei, Q. Yuan and H. Liang, *RSC Adv.*, 2019, **9**, 40845.
8 Y. Li, G. Hou, J. Yang, J. Xie, X. Yuan, H. Yang and M. Wang, *RSC Adv.*, 2016, **6**, 16395.
9 M. J. Chang, W. N. Cul, X. J. Chal, J. Liu, K. Wang and L. Qiu, *J. Mater. Sci.: Mater. Electron.*, 2019, **30**, 1009–1016.
10 R. Zhao, Y. Tian, S. Li, T. Ma, H. Lei and G. Zhu, *J. Mater. Chem. A*, 2019, **7**, 22559.
11 C. Wang, P. Cheng, Y. Yao, Y. Yamauchi, X. Yan, J. Li and J. Na, *J. Hazard. Mater.*, 2020, **392**, 122164.
12 Y. Ren, T. Li, W. Zhang, S. Wang, M. Shi, C. Shan, W. Zhang, X. Guan, L. Lv, M. Hua and B. Pan, *J. Hazard. Mater.*, 2019, **365**, 312–321.
13 J. Xiong, A. Li, Y. Liu, L. Wang, X. Qin and J. Yu, *J. Mater. Chem. A*, 2021, **9**, 21005.
14 O. Shekhah, H. Wang, S. Kowarik, F. Schreiber, M. Paulus, M. Tolan, C. Sternemann, F. Evers, D. Zacher, R. Fischer and C. Wöll, *J. Am. Chem. Soc.*, 2007, **129**, 15118–15119.
15 O. Shekhah, H. Wang, T. Strunskus, P. Cyganik, D. Zacher, R. Fischer and C. Wöll, *Langmuir*, 2007, **23**, 7440–7442.
16 R. Gil-San-Millan, P. Delgado, E. Lopez-Maya, J. D. Martin-Romera, E. Barea and J. A. R. Navarro, *ACS Appl. Mater. Interfaces*, 2021, **13**, 50491–50496.
17 M. da Silva Pinto, C. A. Sierra-Avila and J. P. Hinestroza, *Cellulose*, 2012, **19**, 1771–1779.
18 H. N. Rubin, B. H. Neufeld and M. M. Reynolds, *ACS Appl. Mater. Interfaces*, 2018, **10**, 15189–15199.
19 M. Schelling, M. Kim, E. Otal and J. Hinestroza, *Bioengineering*, 2018, **5**, 14.
20 H. Y. Jang, J. K. Kang, J. A. Park, S. C. Lee and S. B. Kim, *Environ. Pollut.*, 2020, **267**, 115583.
21 L. Lu, C. Hu, Y. Zhu, H. Zhang, R. Li and Y. Xing, *Cellulose*, 2018, **25**, 4223–4238.
22 H. J. Lee, J. Kim and C. H. Park, *Text. Res. J.*, 2014, **84**, 267–278.
23 Y. Liu, D. Thibodeaux, G. Gamble, P. Bauer and D. VanDerveer, *Appl. Spectrosc.*, 2012, **66**, 983–986.
24 S. Lee and C. H. Park, *Text. Res. J.*, 2019, **89**, 2376–2394.
25 X. Z. Guo, S. S. Han, J. M. Yang, X. M. Wang, S. S. Chen and S. Quan, *Ind. Eng. Chem. Res.*, 2020, **59**, 2113–2122.
26 Q. Xu and X. Zhao, *J. Mater. Chem.*, 2012, **22**, 16416–16421.
27 M. S. Khan, M. Khalid and M. Shahid, *Mater. Adv.*, 2020, **1**, 1575.
28 F. Tan, M. Liu, K. Li, Y. Wang, J. Wang, X. Guo, G. Zhang and C. Song, *Chem. Eng. J.*, 2015, **281**, 360–367.
29 Y. Jia, Q. Jin, Y. Li, Y. Sun, J. Huo and X. Zhao, *Anal. Methods*, 2015, **7**, 1463.
30 H. Liu, X. Ren and L. Chen, *J. Ind. Eng. Chem.*, 2016, **34**, 278–285.
31 W. Li, T. Zhang, L. Lv, Y. Chen, W. Tang and S. Tang, *Colloids Surf., A*, 2021, **624**, 126791.
32 F. Mahmoudi, M. M. Amini and M. Sillanpää, *J. Taiwan Inst. Chem. Eng.*, 2020, **116**, 303–313.
33 J. Lee, K. Lee and J. Kim, *ACS Appl. Mater. Interfaces*, 2021, **13**, 1620–1631.
34 M. Nehra, N. Dilbaghi, N. K. Singhal, A. A. Hassan, K. H. Kim and S. Kumar, *Environ. Res.*, 2019, **169**, 229–236.
35 R. M. Abdelhameed, H. Abdel-Gawad, M. Elshahat and H. E. Emam, *RSC Adv.*, 2016, **6**, 42324.
36 H. E. Emam, H. B. Ahmed, E. Gomaa, M. H. Helal and R. M. Abdelhameed, *Cellulose*, 2020, **27**, 7139–7155.
37 H. Zhao, L. Qian, H. Lv, Y. Wang and G. Zhao, *ChemCatChem*, 2015, **7**, 4148–4155.
38 S. Abdpour, E. Kowsari, M. R. A. Moghaddam, L. Schmolke and C. Janiak, *J. Solid State Chem.*, 2018, **266**, 54–62.
39 J. Hang, X. H. Yi, C. C. Wang, H. Fu, P. Wang and Y. Zhao, *J. Hazard. Mater.*, 2022, **424**, 127415.
40 L. Ai, C. Zhang, L. Li and J. Jiang, *Appl. Catal., B*, 2014, **148–149**, 191–200.
41 S. Lu, L. Liu, H. Demissie, G. An and D. Wang, *Environ. Int.*, 2021, **146**, 106273.
42 Y. He, W. Dong, X. Li, D. Wang, Q. Yang, P. Deng and J. Huang, *J. Colloid Interface Sci.*, 2020, **574**, 364–376.
43 J. Yang, X. Niu, S. An, W. Chen, J. Wang and W. Liu, *RSC Adv.*, 2017, **7**, 2943–2952.
44 A. C. Silva, M. R. Almeida, M. Rodriguez, A. R. T. Machado, L. C. A. Oliveira and M. C. Pereira, *J. Photochem. Photobiol., A*, 2017, **332**, 54–59.